Technical Note: Improved partial wavelet coherency for understanding scale-specific and localized bivariate relationships in geosciences

Wei Hu[1] and Bing Si[2]

[1]*The New Zealand Institute for Plant and Food Research Limited, Private Bag 4704, Christchurch 8140, New Zealand*

[2]*University of Saskatchewan, Department of Soil Science, Saskatoon, SK S7N 5A8, Canada*

Correspondence to: Wei Hu (wei.hu@plantandfood.co.nz)

Abstract

Bivariate wavelet coherency is a measure of correlation between two variables in the location-scale (spatial data) or time-frequency (time series) domain. It is particularly suited to geoscience where relationships between multiple variables differ with locations (times) and/or scales (frequencies) because of various processes involved. However, it is well-known that bivariate relationships can be misleading when both variables are dependent on other variables. Partial wavelet coherency (PWC) has been proposed to detect scale-specific and localized bivariate relationships by excluding the effects of other variables, but is limited to one excluding variable and provides no phase information. We aim to develop a new PWC method that can deal with multiple excluding variables and provide phase information. Both stationary and non-stationary artificial datasets with the response variable being the sum of five cosine waves at 256 locations are used to test the method.

The new method was also applied to a free water evaporation dataset. Our results verified the advantages of the new method in capturing phase information and dealing with multiple excluding variables. Where there is one excluding variable, the new method produces higher and more accurate PWC values than the previous PWC calculation that mistakenly used bivariate real coherence rather than bivariate complex coherence in the calculation. We suggest the PWC method is used to untangle scale-specific and localized bivariate relationships after removing the effects of other variables in geosciences. The PWC calculations were coded with Matlab and are freely accessible (https://figshare.com/s/bc97956f43fe5734c784).

1. Introduction

Geoscience data, such as the spatial distribution of soil moisture in undulating terrains and time series of climatic variables, usually consist of a variety of transient processes with different scales or frequencies that may be localized in space or time (Torrence and Compo, 1998; Si, 2008; Graf et al., 2014). For example, time series of air temperature usually fluctuates periodically at different scales (e.g., daily and yearly), but abrupt changes in air temperature (e.g., extremely high or low) may occur at certain time points as a result of extreme weather and climate events (e.g., heat and rain). Wavelet methods are widely used to detect localized features of geoscience data.

Wavelet analyses are based on the wavelet transform using mother wavelet function,

which expands spatial (or time series) data into location-scale (or time-frequency) space for identification of localized intermittent scales (or frequencies). For convenience, we will mainly refer to location and scale irrespective of spatial or time series data unless otherwise mentioned. Bivariate wavelet coherency (BWC) is widely accepted as a tool for detecting scale-specific and localized bivariate relationships in a range of areas in geoscience (Lakshmi et al., 2004; Si and Zeleke, 2005; Das and Mohanty, 2008; Polansky et al., 2010; Biswas and Si, 2011). The BWC partitions correlation between two variables into different locations and scales, which are different from the overall relationships at the sampling scale as shown by the traditional correlation coefficient. For example, BWC analysis indicated that soil water content of a hummocky landscape in the Canadian Prairies was negatively correlated to soil organic carbon content at a slope scale (50 m), but they were positively correlated at a watershed scale (120 m) in summer because of the different processes involved at different scales (Hu et al., 2017b). Because the positive correlation may cancel out with the negative one at different scales and/or locations, the traditional correlation coefficient between soil water content and soil organic carbon content does not differ significantly from zero, which can be misleading.

Recently, Hu and Si (2016) have extended BWC to multiple wavelet coherence (MWC) that can be used to untangle multivariate (≥3 variables) relationships in multiple location-scale domains. This method has been successfully used in hydrology (Hu et al., 2017b; Nalley et al., 2019; Su et al., 2019; Gu et al., 2020; Mares et al., 2020) and other areas such as soil science (Centeno et al., 2020), environmental science (Zhao et al., 2018), meteorology (Song et al., 2020), and economics (Sen et al., 2019). The MWC application

has shown that an increased number of predictor variables does not necessarily explain more variations in the response variable, partly because predictor variables are usually cross-correlated (Hu and Si, 2016). For the same reason, bivariate relationships can be misleading if the predictor variable is correlated with other variables that control the response variable. Partial correlation analysis is one such method to avoid the misleading relationships resulting from the interdependence between predictor and other variables (Kenney and Keeping, 1939). For example, soil water content of the root zone was found to be positively related to grass yield throughout the year in a small watershed on the Chinese Loess Plateau (Hu et al., 2017a). This was because higher grass yield usually coincided with finer soils that usually have higher water holding capacity. After removing the effects of other factors including sand content, partial correlation analysis indicated that soil water content was negatively affected by grass yield during growing seasons and not affected by grass yield during non-growing seasons as expected. The study of Hu et al. (2017a) clearly demonstrated that partial correlation analysis can be an effective method to avoid misleading relationships between response (e.g., soil water content) and predictor variables (e.g., grass yield) when the latter was interdependent with other variables (e.g., sand content). However, the extension of partial correlation to the multiple location-scale domain is limited. In order to better understand the bivariate relationships at various scales and locations, BWC needs to be extended to partial wavelet coherency (PWC) by eliminating the effects of other variables.

BWC was extended to PWC by Mihanović et al. (2009). Their method has been widely used in the areas of marine science (Ng and Chan, 2012a, b), meteorology (Tan et al., 2016;

Rathinasamy et al., 2017), and economics (Aloui et al., 2018; Altarturi et al., 2018a; Wu et al., 2020), as well as in the study of greenhouse gas emissions (Jia et al., 2018; Li et al., 2018; Mutascu and Sokic, 2020), among others. For example, PWC analysis indicated that the Southern Oscillation Index and Pacific Decadal Oscillation did not affect precipitation across India, while this was misinterpreted by the BWC analysis because of their interdependence on Niño 3.4, which affects precipitation (Rathinasamy et al., 2017). Unfortunately, the PWC calculation in many previous studies (Ng and Chan, 2012b; Rathinasamy et al., 2017; Aloui et al., 2018; Altarturi et al., 2018b; Jia et al., 2018; Li et al., 2018; Mutascu and Sokic, 2020; Wu et al., 2020) was based on an incorrect Matlab code developed by Ng and Chan (2012a) who might have misinterpreted the equation of Mihanović et al. (2009) and mistakenly used bivariate real coherence rather than bivariate complex coherence for calculating PWC. Moreover, Mihanović et al. (2009) considered only one excluding variable (i.e., the variable that influences the response variable is excluded) and did not include the phase angle difference between response and predictor variables. The PWC values between response and predictor variables can still be misleading if more than one variable is interdependent with the predictor variable. This is especially true if these variables are correlated with the predictor variable at different locations and/or scales. Without phase information, it is hard to tell if the correlation at a location and scale is positive or negative.

As an extension of previous studies (Mihanović et al., 2009; Hu and Si, 2016), this paper aims to develop a PWC method that considers more than one excluding variable and provides phase information. This new method reveals the magnitude and type of bivariate

106 relationships after removing the effects from all potentially interdependent variables. We
107 expect that the new method produces more accurate PWC values than the calculation of Ng
108 and Chan (2012a) where there is one excluding variable. The new method is an extension
109 of the multivariate partial coherency in the frequency (scale) domain (Koopmans, 1995).
110 The proposed method is first tested with artificial datasets following Yan and Gao (2007)
111 and Hu and Si (2016) to demonstrate its capability of capturing the known relationships of
112 the artificial data. Then it is applied to a real dataset, i.e., time series of free water
113 evaporation at the Changwu site in China (Hu and Si, 2016). Finally, the advantages and
114 weaknesses of the new method are discussed by comparing it with the previous PWC
115 method (Mihanović et al., 2009) and calculation (Ng and Chan, 2012a).

116 ## 2. Theory

117 Wavelet analysis is based on the wavelet transform, which includes continuous wavelet
118 transform and discrete wavelet transform. While the discrete wavelet transform is mainly
119 used for data compression and noise reduction, the continuous wavelet transform is widely
120 used for extracting scale-specific and localized features, as in the case of this study
121 (Grinsted et al., 2004). The wavelet transform decomposes the spatial (or time series) data
122 into a set of location- and scale-specific wavelet coefficients, which are scaled (contracted
123 or expanded) and shifted versions of mother wavelets. Different mother wavelets are
124 available for wavelet transform. Among which, the Morlet wavelet, composed of a complex
125 exponential multiplied by a Gaussian window, provides a good balance between location
126 and scale localization. Therefore, continuous wavelet transform with the Morlet wavelet is

suitable to transform spatial (or time series) data into a location-scale (or time-frequency) domain, which allows us to identify both location-specific amplitude and phase information of wavelet coefficients at different scales (Torrence and Compo, 1998). Wavelet coefficients and their complex conjugates are used to calculate auto-wavelet power spectra and cross-wavelet power spectra. BWC is calculated as the ratio of smoothed cross-wavelet power spectra of two variables to the product of their auto-wavelet power spectra (Grinsted et al., 2004). Hu and Si (2016) extended wavelet coherence from two to multiple (≥3) variables and developed MWC. Detailed information on the calculations of wavelet coefficients, auto- and cross-wavelet power spectra, BWC, and MWC based on the continuous wavelet transform can be found in previous studies (e.g., Torrence and Compo, 1998; Grinsted et al., 2004; Si and Farrell, 2004; Si, 2008; Hu and Si, 2016; Hu et al., 2017b). Here, we will only introduce the theory and calculation that are most relevant to PWC.

Similar to BWC and MWC, PWC is calculated from auto- and cross-wavelet power spectra, for the response variable y, predictor variable x, and excluding variables Z ($Z = \{Z_1, Z_2, \cdots, Z_q\}$). Koopmans (1995) developed the multivariate complex PWC in the frequency (scale) domain. Here, we extend the Koopmans (1995) method from the frequency (scale) domain to the time-frequency (location-scale) domain. Therefore, the complex PWC between y and x after excluding variables Z at scale s and location τ, $\gamma_{y,x\cdot \mathrm{Z}}(s,\tau)$, can be written as

$$\gamma_{y,x\cdot \mathrm{Z}}(s,\tau) = \frac{\left(1 - R^2_{y,x,Z}(s,\tau)\right)\, \gamma_{y,x}(s,\tau)}{\sqrt{\left(1 - R^2_{y,Z}(s,\tau)\right)\left(1 - R^2_{x,Z}(s,\tau)\right)}} \qquad (1)$$

where $R^2_{yx,Z}(s,\tau)$, $R^2_{y,Z}(s,\tau)$, and $R^2_{x,Z}(s,\tau)$ can be calculated by following Hu and Si (2016) as

$$R^2_{y,x,Z}(s,\tau) = \frac{\underset{W}{\leftrightarrow}^{y,Z}(s,\tau)\,\underset{W}{\leftrightarrow}^{Z,Z}(s,\tau)^{-1}\,\overline{\underset{W}{\leftrightarrow}^{x,Z}(s,\tau)}}{\underset{W}{\leftrightarrow}^{y,x}(s,\tau)} \quad (2)$$

$$R^2_{y,Z}(s,\tau) = \frac{\underset{W}{\leftrightarrow}^{y,Z}(s,\tau)\,\underset{W}{\leftrightarrow}^{Z,Z}(s,\tau)^{-1}\,\overline{\underset{W}{\leftrightarrow}^{y,Z}(s,\tau)}}{\underset{W}{\leftrightarrow}^{y,y}(s,\tau)} \quad (3)$$

$$R^2_{x,Z}(s,\tau) = \frac{\underset{W}{\leftrightarrow}^{x,Z}(s,\tau)\,\underset{W}{\leftrightarrow}^{Z,Z}(s,\tau)^{-1}\,\overline{\underset{W}{\leftrightarrow}^{x,Z}(s,\tau)}}{\underset{W}{\leftrightarrow}^{x,x}(s,\tau)} \quad (4)$$

Eq. (1) can be also derived analogously from the complex partial spectrum for the frequency domain according to the definition of complex coherence between two variables in the time-frequency domain (see the Supplement (Sect. S1) for the derivation process). Note that $R^2_{y,x,Z}(s,\tau)$ is a matrix with complex values, while $R^2_{y,Z}(s,\tau)$ and $R^2_{x,Z}(s,\tau)$ are matrices with real numbers. $\gamma_{y,x}(s,\tau)$ is the complex wavelet coherence between y and x, which can be written as

$$\gamma_{y,x}(s,\tau) = \frac{\underset{W}{\leftrightarrow}^{y,x}(s,\tau)}{\left(\underset{W}{\leftrightarrow}^{y,y}(s,\tau)\underset{W}{\leftrightarrow}^{x,x}(s,\tau)\right)^{1/2}} \quad (5)$$

where $\underset{(\cdot)}{\leftrightarrow}$ is the smoothing operator, $\overline{(\cdot)}$ is the complex conjugate operator, $(\cdot)^{-1}$ indicates the inverse of the matrix, and

$$\underset{W}{\leftrightarrow}^{y,Z}(s,\tau) = \left[\underset{W}{\leftrightarrow}^{y,Z_1}(s,\tau)\,\underset{W}{\leftrightarrow}^{y,Z_2}(s,\tau)\cdots\underset{W}{\leftrightarrow}^{y,Z_q}(s,\tau)\right] \quad (6)$$

$$\underset{W}{\leftrightarrow}^{x,Z}(s,\tau) = \left[\underset{W}{\leftrightarrow}^{x,Z_1}(s,\tau)\,\underset{W}{\leftrightarrow}^{x,Z_2}(s,\tau)\cdots\underset{W}{\leftrightarrow}^{x,Z_q}(s,\tau)\right] \quad (7)$$

$$\underset{W}{\overleftrightarrow{}}^{Z,Z}(s,\tau)=\begin{bmatrix}\underset{W}{\overleftrightarrow{}}^{Z_1,Z_1}(s,\tau) & \cdots & \underset{W}{\overleftrightarrow{}}^{Z_1,Z_q}(s,\tau)\\ \vdots & \ddots & \vdots\\ \underset{W}{\overleftrightarrow{}}^{Z_q,Z_1}(s,\tau) & \cdots & \underset{W}{\overleftrightarrow{}}^{Z_q,Z_q}(s,\tau)\end{bmatrix} \quad (8)$$

where $\underset{W}{\overleftrightarrow{}}^{A,B}(s,\tau)$ is the smoothed auto-wavelet power spectra (when A=B) or cross-wavelet power spectra (when $A\neq B$) at scale s and location τ, respectively.

The squared PWC (hereinafter referred to as PWC) at scale s and location τ, $\rho^2_{y,x\cdot Z}$, can be written as

$$\rho^2_{y,x\cdot Z}=\frac{\left|1-R^2_{y,x,Z}(s,\tau)\right|^2 R^2_{y,x}(s,\tau)}{\left(1-R^2_{y,Z}(s,\tau)\right)\left(1-R^2_{x,Z}(s,\tau)\right)} \quad (9)$$

where $R^2_{y,x}(s,\tau)$ is squared BWC between y and x, which can be expressed as

$$R^2_{y,x}(s,\tau)=\frac{\underset{W}{\overleftrightarrow{}}^{y,x}(s,\tau)\overline{\underset{W}{\overleftrightarrow{}}^{y,x}(s,\tau)}}{\underset{W}{\overleftrightarrow{}}^{y,y}(s,\tau)\underset{W}{\overleftrightarrow{}}^{x,x}(s,\tau)} \quad (10)$$

The phase angle (i.e., angle between two complex numbers) between y and x after excluding effect of Z is

$$\vartheta_{y,x\cdot Z}(s,\tau)=\varphi_{y,x\cdot Z}(s,\tau)+\vartheta_{y,x}(s,\tau) \quad (11)$$

where

$$\varphi_{y,x\cdot Z}(s,\tau)=\arg\left(1-R^2_{y,x,Z}(s,\tau)\right) \quad (12)$$

and $\vartheta_{y,x}(s,\tau)$ is the wavelet phase between y and x, which can be expressed as

$$\vartheta_{y,x}(s,\tau)=\tan^{-1}\left(\mathrm{Im}\left(W^{y,x}(s,\tau)\right)/\mathrm{Re}\left(W^{y,x}(s,\tau)\right)\right) \quad (13)$$

where arg denotes the argument of the complex number, $W^{y,x}(s,\tau)$ is the cross-wavelet

179 power spectrum between y and x at scale s and location τ; Im and Re denote the
180 imaginary and real part of $W^{y,x}(s,\tau)$, respectively.

181 When only one variable (e.g., $Z1$) is excluded, Eq.(9) can be written as (see the
182 Supplement (Sect. S2) for the derivation process)

183 $$\rho^2_{y,x\cdot Z1} = \frac{\left|\gamma_{y,x}(s,\tau) - \gamma_{y,Z1}(s,\tau)\overline{\gamma_{x,Z1}(s,\tau)}\right|^2}{\left(1-R^2_{y,Z1}(s,\tau)\right)\left(1-R^2_{x,Z1}(s,\tau)\right)} \quad (14)$$

184 The widely used Monte Carlo method (Torrence and Compo, 1998; Grinsted et al., 2004;
185 Si and Farrell, 2004) is used to calculate PWC at the 95% confidence level. In brief, the
186 PWC calculation is repeated for a sufficient number (i.e., minimum number required) of
187 times using data generated by Monte Carlo simulations based on the first-order
188 autocorrelation coefficient (r1). The first-order autoregressive model (AR(1)) is chosen
189 because most geoscience data can be effectively simulated by it (Wendroth et al., 1992;
190 Grinsted et al., 2004; Si and Farrell, 2004), although we recognize that time series with
191 long-range dependence is also common in many areas such as hydrology (Szolgayová et
192 al., 2014). Different combinations of r1 values (i.e., 0.0, 0.5, and 0.9) were used to generate
193 10 to 10 000 AR(1) series with three, four and five variables. Our results indicate that the
194 noise combination has little impact on the PWC values at the 95% confidence level as also
195 found by Grinsted et al. (2004) for the BWC case (data not shown). The relative difference
196 of PWC at the 95% confidence level compared with that calculated from the 10 000 AR(1)
197 series decreases with the increase in number of AR(1) series (Fig. S1 of Sect. S3 in the
198 Supplement). When the number of AR(1) is above 300, a very low maximum relative

199 difference (e.g., <2%) is observed. Therefore, a repeating number of 300 seems to be
200 sufficient for a significance test. However, if calculation time is not a barrier, a higher
201 repeating number, such as ≥1000, is recommended. The 95th percentile of PWCs of all
202 simulations at each scale represents PWC at the 95% confidence level. The average PWC,
203 percent area of significant coherence (PASC) relative to the whole wavelet location–scale
204 domain (Hu and Si, 2016), and average value of significant PWC (PWC_{sig}) are also
205 calculated for different location–scale domains.

206 In the case of one excluding variable ($Z = \{Z_1\}$), Mihanović et al. (2009) suggested that
207 PWC can be calculated by an equation analogous to the traditional partial correlation
208 squared (Kenney and Keeping, 1939) without giving detailed derivation process. Their
209 equation is the same as Eq. (14). Unfortunately, Ng and Chan (2012a) might have
210 misinterpreted the equation of Mihanović et al. (2009) and developed Matlab code for
211 calculating PWC using the equation expressed as

212 $$\rho^2_{y,x\cdot Z1} = \frac{\left|R_{y,x}(s,\tau) - R_{y,Z1}(s,\tau)\, R_{x,Z1}(s,\tau)\right|^2}{\left(1-R^2_{y,Z1}(s,\tau)\right)\left(1-R^2_{x,Z1}(s,\tau)\right)} \quad (15)$$

213 where $R_{y,x}(s,\tau)$, $R_{y,Z1}(s,\tau)$, and $R_{x,Z1}(s,\tau)$ are the square root of $R^2_{y,x}(s,\tau)$,
214 $R^2_{y,Z1}(s,\tau)$, $R^2_{x,Z1}(s,\tau)$, respectively. $R^2_{y,Z1}(s,\tau)$ and $R^2_{x,Z1}(s,\tau)$ can be calculated from
215 Eq. (10) by replacing y and x with their corresponding variables. Eq. (15) has been
216 widely used to calculate PWC in the case of one excluding variable (Ng and Chan, 2012b;
217 Rathinasamy et al., 2017; Aloui et al., 2018; Altarturi et al., 2018b; Jia et al., 2018; Li et al.,
218 2018; Mutascu and Sokic, 2020; Wu et al., 2020). Note that complex coherence and real

coherence are involved in the numerators of Eqs. (14) and (15), respectively, while the denominators are exactly the same. Further comparison indicates that Eq. (15) underestimates PWC value relative to Eq. (14) unless $\gamma_{y,x}(s,\tau)$ and $\gamma_{y,Z1}(s,\tau)\,\overline{\gamma_{x,Z1}(s,\tau)}$ in Eq. (14) are collinear (i.e., their arguments are identical) under which the two equations produce the same PWC values. Differences between Eqs. (14) and (15) will be discussed further using both artificial data and a real dataset. For comparison purposes, we refer to Eqs. (14) and (15) as the new calculation and the classical calculation, respectively.

3. Method test using artificial data

3.1 Artificial data and analysis

PWC is first tested using the cosine-like artificial dataset produced following Yan and Gao (2007). The cosine-like artificial datasets are suitable for testing the new method because they mimic many spatial or time series data in geoscience such as climatic variables, hydrologic fluxes, seismic signals, El Niño-Southern Oscillation, land surface topography, ocean waves, and soil moisture. The procedures to test PWC are largely based on Hu and Si (2016), where the same dataset has been used to test the MWC method (refer to Hu and Si (2016) for a detailed description of the artificial dataset). The response variable (y and z for the stationary and non-stationary case, respectively) is the sum of five cosine waves (y_1 to y_5 and z_1 to z_5 for the stationary and non-stationary case, respectively) at 256 locations (Hu and Si, 2016). For y_1 to y_5, they have consistent dimensionless scales of 4, 8, 16, 32, and 64, respectively, across the series. From z_1 to z_5, the dimensionless scales gradually change with location, with the maximum dimensionless scales of 4, 8, 16, 32, and 64,

240 respectively. The variance of the response variable y and z is 2.5. All other variables are
241 orthogonal to each other with equal variance of 0.5. The predictor and excluding variables
242 (Fig. S1 of Sect. S4 in the Supplement) are selected from two of the five cosine waves (i.e.,
243 y_2 and y_4 or z_2 and z_4) and/or their derivatives. The exact variables and procedures to test
244 the new PWC method are explained below.

245 First, PWC between response variable y (or z) and predictor variable, i.e., y_2 (or z_2), is
246 calculated after excluding the effect of one variable. Four types of excluding variable are
247 involved (Fig. S2 of Sect. S4 in the Supplement): (a) original series of y_4 (or z_4); (b) second
248 half of the original series of y_2 (or z_2) are replaced by 0 to simulate abrupt changes (i.e.,
249 transient and localized feature) of the spatial data. They are referred to as y_2h_0 (*or* z_2h_0); (c)
250 white noises with zero-mean and standard deviations of 0.3 (weak noise), 1 (moderate
251 noise), and 4 (high noise) are added to y_2 (or z_2) as suggested by Hu and Si (2016) to
252 simulate non-perfect cyclic patterns of the excluding variables. They are referred to as y_2wn
253 (*or* z_2wn), y_2mn (*or* z_2mn), and y_2sn (*or* z_2sn), respectively; and (d) a combination of type b
254 and type c. They are referred to as y_2wnh_0 (*or* z_2wnh_0), y_2mnh_0 (*or* z_2mnh_0), and y_2snh_0 (*or*
255 z_2snh_0), respectively.

256 Second, PWC between response variable y (or z) and predictor variable, i.e., y_2y_4 (sum
257 of y_2 and y_4) for the stationary case or z_2z_4 (sum of z_2 and z_4) for the non-stationary case, is
258 calculated with two excluding variables, which is a combination of y_4 (or z_4) and y_2 (or z_2)
259 or its noised series (y_2wn *or* z_2wn, y_2mn *or* z_2mn, and y_2sn *or* z_2sn).

260 The merit of the artificial data is that we know the exact scale-specific and localized

bivariate relationships after the effect of excluding variables is removed. Theoretically, we expect (a) PWC is 1 at scales corresponding to relative complement of excluding variable scales in predictor variable scales, and 0 at other scales. For example, PWC between y and y_2y_4 after excluding the effect of y_4 is expected to be 1 at the scale of 8, which is the relative complement of scale of excluding variable y_4 (32) in scales of predictor variable y_2y_4 (8 and 32), and 0 at other scales; (b) PWC remains 1 at the second half of series where spatial series is replaced by 0, and 0 at the first half of the original series. For example, PWC between y and y_2 after excluding the effect of y_2h_0 is expected to be 0 and 1 at the first and second half of series, respectively, at the scale of 8; and (c) PWC increases as more noises are included in the excluding variables. For example, PWC between y and y_2 after excluding the effect of noised series of y_2 is expected to increase with increasing noises in an order of $y_2sn>y_2mn>y_2wn$ at the scale of 8.

3.2 PWC with artificial data

3.2.1 PWC with one excluding variable using the new method

Fig. 1 shows PWC between response variable y (or z) and predictor variable y_2 (or z_2) by excluding one variable. For the stationary case, there is one horizontal band (red color) representing an in-phase high PWC value at scales around 8 for all locations after eliminating the effect of y_4 (Fig. 1a). Note that the PWC values between y and y_2 after excluding the effect of y_4 are not exactly 1 as would be expected at all location-scale domains, because of the effect of smoothing along locations and scales. However, the PWC values at the center of the significance band, which corresponds to the predictor variable y_2

at exactly the scale of 8, are very close to 1 (0.996), and the mean PWC_{sig} values are very high (i.e., 0.96). The result is similar to the BWC between y and y_2 (data not shown). This is understandable because y_4 is orthogonal to y_2, and excluding the effect of y_4 does not affect the relationship between y and y_2 at all.

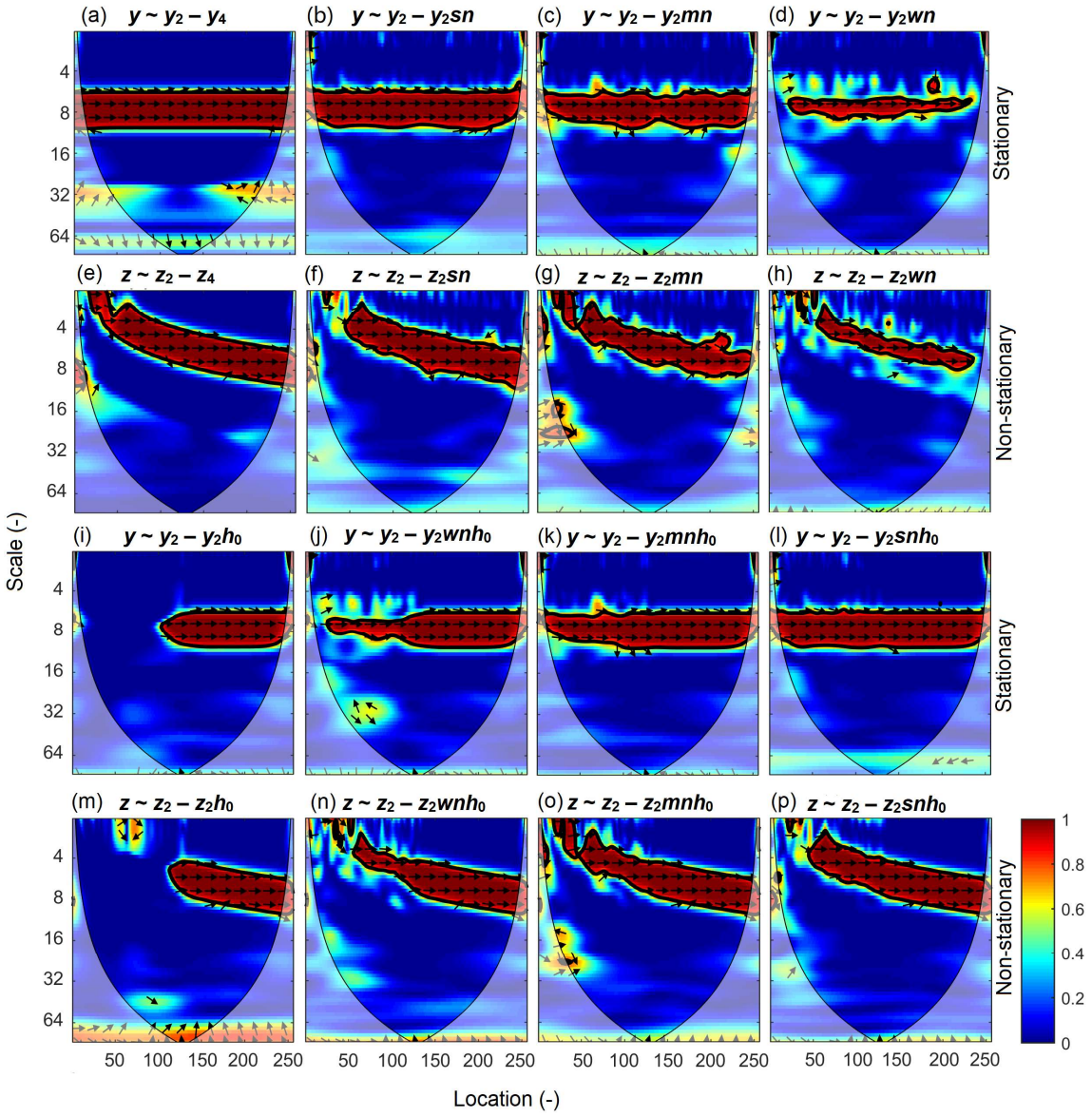

Figure 1.

Partial wavelet coherency (PWC) between response variable y (or z) and predictor variable

289 y_2 (or z_2) after excluding the effect of variables y_4 (or z_4), y_2sn (or z_2sn), y_2mn (or z_2mn),
290 y_2wn (or z_2wn), y_2h_0 (or z_2h_0), y_2wnh_0 (or z_2wnh_0), y_2mnh_0 (or z_2mnh_0), and y_2snh_0 (or z_2snh_0)
291 for the stationary (or non-stationary) case using the new method. Arrows represent the
292 phase angles of the cross-wavelet power spectra between two variables after eliminating
293 the effect of excluding variables. Arrows pointing to the right (left) indicate positive
294 (negative) correlations. Thin and thick solid lines show the cones of influence and the 95%
295 confidence levels, respectively. All variables were generated by following Yan and Gao
296 (2007) and Hu and Si (2016) and are explained in Sect. 3.1 and shown in Fig. S2 of Sect.
297 S3 in the Supplement.

298 Compared with the case of excluding variable of y_4 (Fig. 1a), excluding the effect of y_2sn
299 (Fig. 1b) results in slightly narrower band of significant PWC and slightly reduced mean
300 PWC_{sig} (0.94 versus 0.96). When less noise is included in the excluding variables (i.e., y_2mn
301 and y_2wn) (Fig. 1c-d), the significant PWC band becomes narrower. The PASC values are
302 86%, 77%, and 32% for excluding y_2sn, y_2mn and y_2wn, respectively, at scales of 6–10.
303 Moreover, the mean PWC_{sig} decreases from 0.94 (y_2sn) to 0.93 (y_2mn) and 0.89 (y_2wn) when
304 progressively less noise is added (Fig. 1b-d). For the non-stationary case, similar results are
305 obtained (Fig. 1e-h). The only difference is that the scales with significant PWC values
306 change with location, as is found for MWC (Hu and Si, 2016).

307 When the second half of the excluding variable series is replaced by 0, the PWC values
308 in that half are close to 1, while those in the first half of data series are 0 at scales
309 corresponding to the predictor variable (Fig. 1i and 1m). For the stationary case, after
310 excluding the effect of y_2h_0, the PWC values are close to 1 (0.98) and 0 in the second and
311 first half of the data series, respectively, at the dimensionless scale of 8 (Fig. 1i). Similar
312 results are observed for the non-stationary case (Fig. 1m). This is anticipated because the

series of 0s is independent of the predictor variable and hence has no effect on the correlations between response and predictor variables at these locations. If different magnitudes of noises are added to the first half of the excluding variables (y_2 or z_2), the significant PWC band in the first half becomes wider as the magnitude of noises increases, while the significant PWC band in the second half remains almost unchanged (Fig. 1j-l and Fig. 1n-p). In the stationary case, for example, the PASC values at scales of 6–10 are 40% (y_2wnh_0), 74% (y_2mnh_0), and 86% (y_2snh_0) in the first half, while those values vary from 86% to 90% in the second half (Fig. 1j-l). Meanwhile, the mean PWC_{sig} in the first half at scales of 6–10 increases from 0.91 to 0.94 in both the stationary (Fig. 1j-l) and non-stationary (Fig. 1n-p) cases as more noises are added to the excluding variable y_2 or z_2. This indicates that the new PWC method can also capture the abrupt changes (Fig. 1i and 1m) in the data series, and has the ability to deal with localized relationships.

3.2.2 PWC with two excluding variables using the new method

When both y_2 and y_4 (or z_2 and z_4) are considered in the predictor variables, there are two bands of wavelet coherence of 1 between y (or z) and y_2y_4 (or z_2z_4) (Hu and Si, 2016), which correspond to the scales of two predictor variables. However, after the effect of y_4 (or z_4) is removed, only one band with PWC of around 1 occurs at the scale of the predictor variable y_2 (or z_2) (Fig. 2a and 2f). After both predictor variables y_2 and y_4 (or z_2 and z_4) are excluded (Fig. 2b and 2g), PWC between y (or z) and y_2y_4 (or z_2z_4) is 0 at all location-scale domains as expected. When one of the excluding variables y_2 (or z_2) is added with noises, the relationship between response variable y (or z) and predictor variable y_2y_4 (or z_2z_4) becomes

significant at scales of the excluding variable y_2 (or z_2) (Fig. 2c and 2h). Similar to the case of one excluding variable (Fig. 1), less noise in the excluding variable of y_2 (or z_2) results in a narrower significant PWC band, and reduced mean PWC_{sig} values, e.g., from 0.96 (y_2sn) to 0.90 (y_2wn) in the stationary case (Fig. 2c-e) and from 0.95 (z_2sn) to 0.92 (z_2wn) in the non-stationary case (Fig. 2h-j).

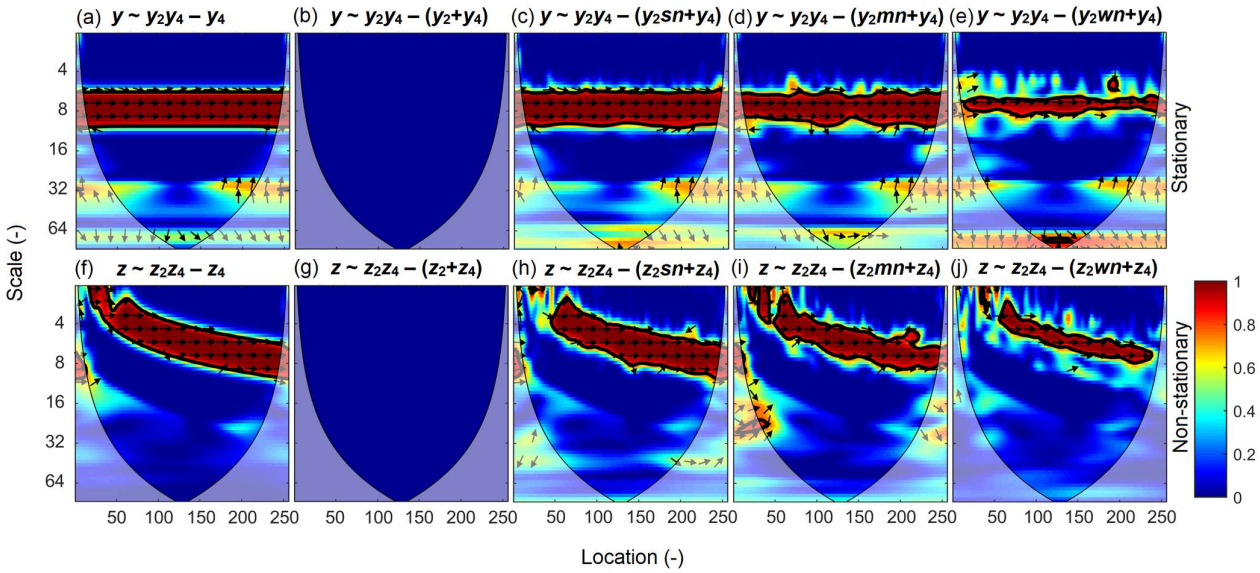

Figure 2.

Partial wavelet coherency (PWC) between response variable y (or z) and predictor variable y_2y_4 (or z_2z_4) after excluding the effect of variables y_4 (or z_4), y_2+y_4 (or z_2+z_4), y_2sn+y_4 (or z_2sn+z_4), y_2mn+y_4 (or z_2mn+z_4), and y_2wn+y_4 (or z_2wn+z_4) for the stationary (or non-stationary) case using the new method. All variables were generated by following Yan and Gao (2007) and Hu and Si (2016) and are explained in Sect. 3.1 and shown in Fig. S2 of Sect. S3 in the Supplement.

4. Method application with real dataset

4.1 Description of free water evaporation dataset

The free water evaporation dataset was used to test MWC (Hu and Si, 2016). In brief, this dataset includes monthly free water evaporation (E), mean temperature (T), relative humidity (RH), sun hours (SH), and wind speed (WS) between January 1979 and December 2013 at Changwu site in Shaanxi province provided by the China Meteorological Administration. During this period, the average daily temperature was 9.4 °C, the average annual rainfall was 571 mm and annual potential evapotranspiration was 883 mm. Because of its location between semi-arid and subhumid climates, agricultural production at the Changwu site is constrained by water availability. Results of wavelet power spectrum of E and BWC between every two variables are shown in Fig. S3 and Fig. S4 (Sect. S3 in the Supplement), respectively.

4.2 PWC with free water evaporation dataset

The PWC analysis indicates that the correlations between E and T after excluding the effect of each of other three variables (RH, SH, and WS) were almost the same as those indicated by BWC (Fig. 3a-c and Fig. S4 of Sect. S3 in the Supplement). For example, E and T, after excluding the effect of RH, were positively correlated at the medium scales (8–32 months). The PASC was 61% and mean PWC_{sig} value was 0.94. No significant correlations between E and T from 1979 to 1992 were found at scales around 64 months after eliminating the influence of RH (Fig. 3a-c). This implies that the influence of mean

temperature on E at these scales and years may be associated with the negative influence of RH on both E and T (Fig. S4 of Sect. S3 in the Supplement).

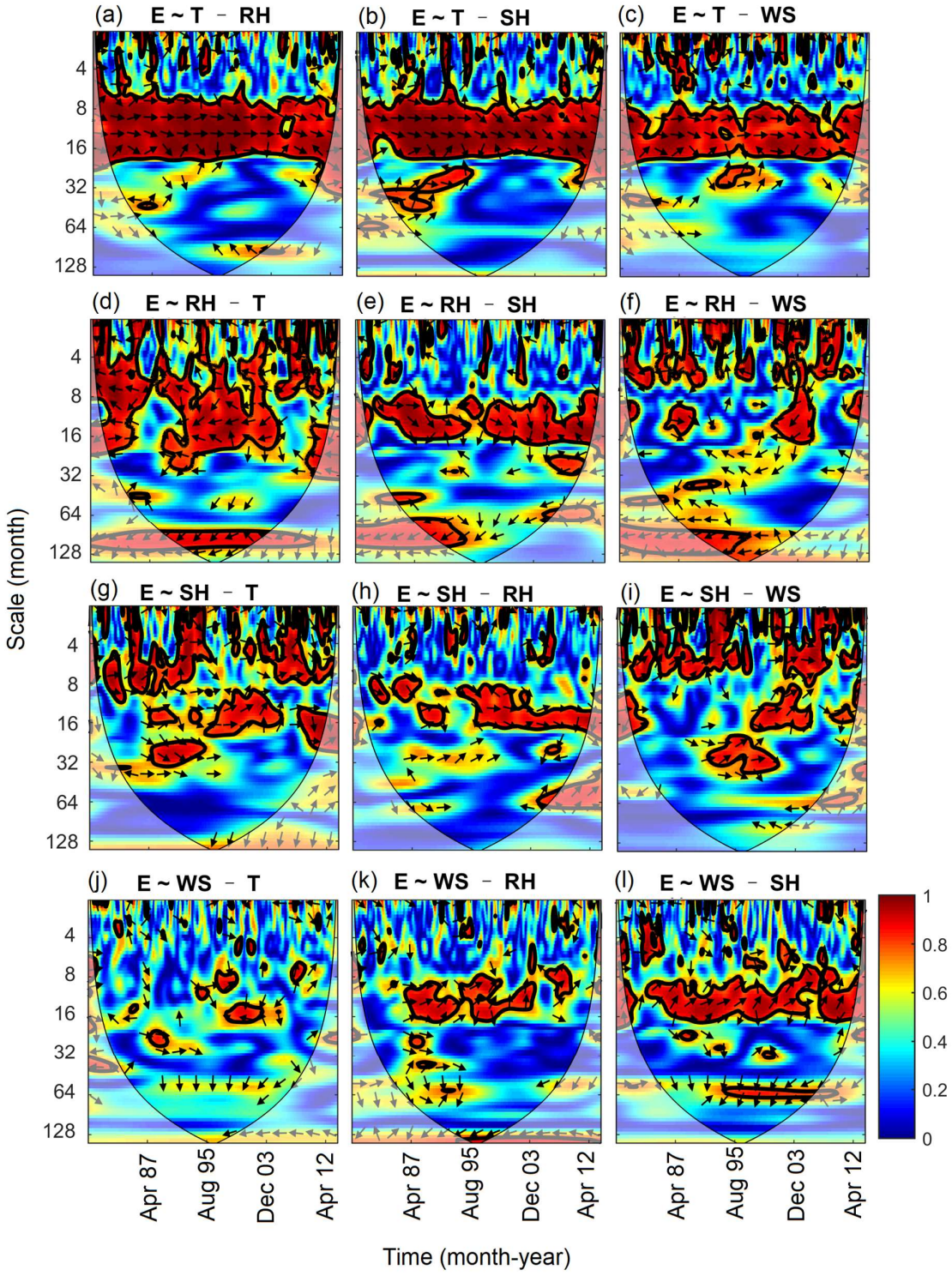

Figure 3.

Partial wavelet coherency (PWC) between evaporation (E) and each meteorological factor (T, mean temperature; RH, relative humidity; SH, sun hours; WS, wind speed) after excluding the effect of each of other three meteorological factors.

PWC between E and RH depended on the excluding variable and scale (Fig. 3d-f). The mean PWC and PASC between E and RH after excluding T were 0.60 and 34%, respectively, which are comparable with the mean BWC (0.62) and PASC (40%) between E and RH. The corresponding values after excluding SH and WS were 0.50 and 0.53 (PWC), 22% and 21% (PASC), respectively. In addition, compared with the BWC between E and RH (Fig. S4 of Sect. S3 in the Supplement), correlations between E and RH were weak at small scales (<8 months) and medium scales (8–32 months) after eliminating the influence of SH and WS (Fig. 3e-f), respectively. Therefore, excluding the variable of T had less influence on the coherence between E and RH compared with excluding the variables of SH and WS. This is mainly because RH and T are correlated with E at different scales (Fig. S4 of Sect. S3 in the Supplement), i.e., mean temperature affected E mainly at medium scales, while RH affected E across all scales. However, the domain where SH and WS were correlated with E was a subset of that where RH and E were correlated (Fig. S4 of Sect. S3 in the Supplement).

The relationships between E and SH after excluding the other three factors were less consistent (Fig. 3g-h). The areas with significant corrections were scattered over the whole location-scale domain but differed with excluding factor. The PASC varied from 12% (excluding RH) to 20% (excluding T and WS), which is much lower than the PASC (28%)

392 in the case of BWC. The significant relationships between E and WS were only limited to
393 very small areas except for the case of SH being excluded, where E and WS were positively
394 correlated at scales of 8–16 months most of the time (Fig. 3j-l).

395 In general, the PASC decreased after excluding the effects of more factors (data not
396 shown). The correlations between E and each variable after eliminating the effects of all
397 other variables are shown in Fig. 4. The correlations between E and T were still significant
398 at the medium scales (8–32 months) (Fig. 4a), where PASC value was 52% with mean
399 PWC_{sig} of 0.92. The E was still correlated with RH at large scales (>85 months) (Fig. 4b),
400 where PASC value was 35% with mean PWC_{sig} of 0.96. Interestingly, the domain with
401 significant correlation between E and SH and WS was very limited (Fig. 4c-d). This
402 indicates that the influences of SH and WS on E have already been covered by RH and T.
403 This is in agreement with the MWC results that RH and T were the best to explain E
404 variations at all scales (Hu and Si, 2016). Although the RH had the greatest mean wavelet
405 coherence and PASC at the entire location-scale domains, the PWC analysis seems to
406 support that mean temperature was the most dominating factor for free water evaporation
407 at the 1-year cycle (8–16 months), which is the dominant scale of E variation (Fig. S3 of
408 Sect. S3 in the Supplement).

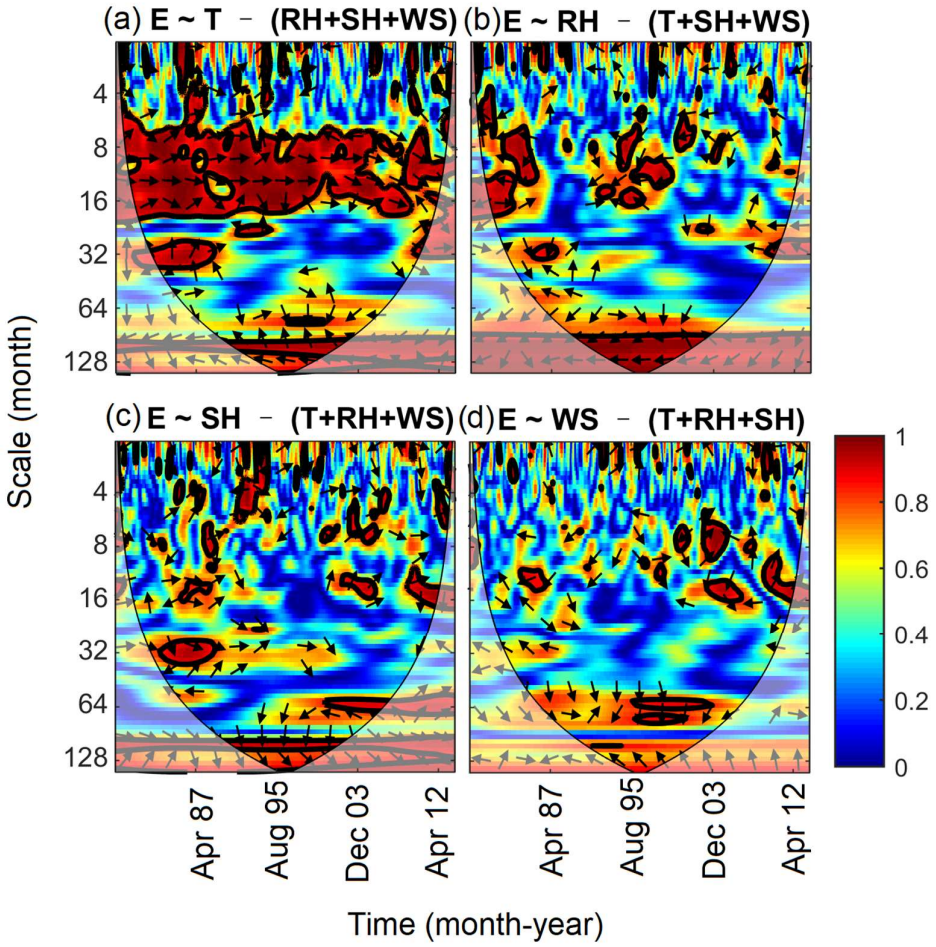

409

410 **Figure 4.**

411 Partial wavelet coherency (PWC) between evaporation (E) and each meteorological factor
412 (T, mean temperature; RH, relative humidity; SH, sun hours; WS, wind speed) after
413 excluding the effects of all other three factors.

414 **5. Discussion on the advantages and weaknesses of the new method**

415 **5.1 Advantages**

416 We extend the partial coherence method from the frequency (scale) domain (Koopmans,
417 1995) to the time-frequency (location-scale) domain. The new method is an extension of

418 previous work on PWC and MWC (Mihanović et al., 2009; Hu and Si, 2016). The method
419 test and application have verified that it has the advantage of dealing with more than one
420 excluding variable and providing the phase information associated with PWC. In the case
421 of one excluding variable, Mihanović et al. (2009) has suggested to calculate PWC by using
422 an equation analogous to the traditional partial correlation squared (Eq. 14), which can be
423 derived from our Eq. (9). However, their equation was, unfortunately, widely used by
424 replacing the complex coherence in Eq. (14) with real coherence as expressed in Eq. (15)
425 (Ng and Chan, 2012b, a; Rathinasamy et al., 2017; Aloui et al., 2018; Altarturi et al., 2018b;
426 Jia et al., 2018; Li et al., 2018; Mutascu and Sokic, 2020; Wu et al., 2020). This mistake is
427 corrected in this paper.

428 The differences between the new calculation (Eq.14) and the classical calculation (Eq.
429 15) are compared in the case of one excluding variable using both the artificial and real
430 datasets. Except for the phase information, the two calculations generally produce
431 comparable coherence for the artificial dataset (Fig. S5 of Sect. S3 in the Supplement).
432 However, the new calculation produces consistently and slightly higher coherence than the
433 classical calculation. For example, their mean PWCs between y and y_2 at the scale of 8 after
434 excluding the effect of y_4 are 1.00 and 0.97, respectively. This indicates that the new
435 calculation produces coherence between y and y_2 at the scale (8) of y_2 closer to 1 as we
436 expect. While the classical calculation produces similar PWC between E and other
437 meteorological factors in most cases especially for the coherence between E and T after
438 excluding the effects of others (Fig. S6 of Sect. S3 in the Supplement), large differences
439 between these two calculations can also be observed. For example, while the new

calculation recognizes the strong coherence between E and RH after excluding the effect of T at scales of around 1 year (Fig. 3d), this coherence was negligible by the classical calculation (Fig. 5a). Mean PWC values by the new calculation were consistently higher than the classical calculation, and the differences ranged from 0.4 to 0.6 around the scale of 1 year (Fig. 5b). Considering the real coherence (Eq.15) rather than complex coherence (Eq.14) between every two variables in the numerators can potentially result in large underestimation of the partial wavelet coherence. Therefore, the ability of the new method and calculation to produce more accurate results than the classical calculation is one of its advantages.

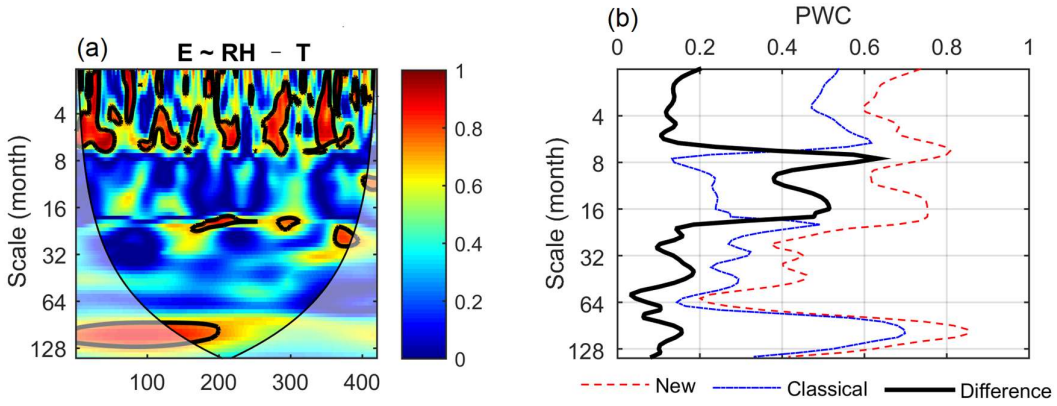

Figure 5.

Partial wavelet coherency (PWC) between evaporation (E) and relative humidity (RH) after excluding the effect of mean temperature (T) using the classical calculation (Eq. 15) (a) and differences in PWC between the new calculation (Eq.14) and classical calculation as a function of scale (b).

Compared with the Mihanović et al. (2009) method, the additional phase information

from the new PWC is another advantage of this new method. This is because phase information is directly related to the type of correlation, i.e., in-phase and out-of-phase indicating positive and negative correlation, respectively. Different types of correlations were usually found at different locations and scales (Hu et al., 2017b). The phase information helps understand the differences in associated mechanisms or processes at different locations and scales. In addition, the phase information will allow us to detect the changes in not only the degree of correlation (i.e., coherence) but also the type of correlation after excluding the effect of other variables. For example, E and RH were positively correlated at the 1-year cycle (8–16 months) from year 1979 to 1995. This is because higher evaporation usually occurs in summer when high T coincides with high RH as influenced by the monsoon climate in the study area (Fig. S4 of Sect. S3 in the Supplement). Interestingly, after excluding the effect of T, E was negatively correlated with RH at the scale of 1 year as we expect (Fig. 3d).

Moreover, our new PWC method applies to cases with more than one excluding variable, which is a knowledge gap. When multiple variables are correlated with both the predictor and response variables, the correlations between predictor and response variables may be misleading if the effects of all these multiple variables were not removed. For example, at the dominant scale (i.e., 1 year) of E variation, contrasting effects of RH on E existed after excluding the effects of T (negative) or SH (positive) (Fig. 3d-e). However, after the effects of all other variables were excluded, there were negligible effects of RH on E at this scale (Fig. 4b). In this case, the relationship between E and RH at the scale of 1 year can be misleading after removing the effects of only one variable. In addition, the dominant role

of mean temperature in driving free water evaporation at the 1-year cycle was proved by removing the effects of all other meteorological factors (Fig. 4a). This also further verifies the suitability of the Hargreaves model (only air temperature and incident solar radiation required) (Hargreaves, 1989) for estimating potential evapotranspiration on the Chinese Loess Plateau (Li, 2012).

5.2 Weaknesses

The new method has the risk to produce spurious high correlations after excluding the effect from other variables. Take the artificial dataset for example, at the scale of 32, PWC values between y and y_2 after excluding y_4 are not significant, but relatively high, partly because of small octaves per scale (octave refers to the scaled distance between two scales with one scale being twice or half of the other, default of 1/12). This spurious unexpected high PWC is caused by low values in both the numerator (partly associated with the low coherence between response y and predictor variables y_2 at the scale of 32) and denominator (partly associated with the high coherence between response y and excluding variable y_4 at the scale of 32) in Eq. (9). The same problem also exists in the classical calculation (Fig. S5 of Sect. S3 in the Supplement). So, caution should be taken to interpret those results. However, it seems that the domain with spurious correlation calculated by the new method is very limited and it is located mainly outside of the cones of influence. Moreover, the unexpected results can be easily ruled out with knowledge of BWC between response and predictor variables. It is expected that the correlation between two variables should not increase after excluding one or more variables. Therefore, BWC analysis is suggested for

499 better interpretation of the PWC results.

500 Similar to BWC and MWC, the confidence level of PWC calculated from the Monte
501 Carlo simulation is based on a single hypothesis testing. But in reality, the confidence level
502 of PWC values at all locations and scales needs to be tested simultaneously. Therefore, the
503 significance test has the problem of multiple testing, i.e., more than one individual
504 hypothesis is tested simultaneously (Schaefli et al., 2007; Schulte et al., 2015). The new
505 method may benefit from a better statistical significance testing method. Options for
506 multiple testing can be the Bonferroni adjusted *p* test (Westfall and Young, 1993) or false
507 discovery rate (Abramovich and Benjamini, 1996; Shen et al., 2002), which is less stringent
508 than the former. The AR(1) model was used to generate noise series for testing the
509 confidence level of PWC. High-order autoregressive models rather than AR(1) may be
510 beneficial for a significance test where spatial (or time series) data are characterized by
511 long-range dependence (Szolgayová et al., 2014).

512 **6. Conclusions**

513 Partial wavelet coherency (PWC) is developed to investigate scale-specific and localized
514 bivariate relationships after excluding the effect of one or more variables in geoscience.
515 Method tests using stationary and non-stationary artificial datasets verified the known
516 scale- and localized bivariate relationships after eliminating the effects of other variables.
517 Compared with the previous PWC method, the new PWC method has the advantage of
518 dealing with more than one excluding variable and providing the phase information (i.e.,
519 correlation type) associated with PWC. In the case of one excluding variable, this new

method produces more accurate coherence than the previous PWC calculation that considered only real coherence rather than complex coherence between every two variables. Application of the new method to the real dataset has further proved its robustness in untangling the bivariate relationships after removing the effects of all other variables in multiple location-scale domains. The new method provides a much needed data-driven tool for unraveling underlying mechanisms in both temporal and spatial data. Thus, combining with wavelet transform, BWC, and MWC, the new PWC method can be used to analyze various processes in geoscience, such as stream flow, droughts, greenhouse gas emissions (e.g., N_2O, CO_2, and CH_4), atmospheric circulation, and oceanic processes (e.g., EI Niño-Southern Oscillation).

Code/Data availability

The Matlab codes for calculating PWC, along with the updated MWC codes, are freely accessible (https://figshare.com/s/bc97956f43fe5734c784). The codes are developed based on those provided by Aslak Grinsted (http://www.glaciology.net/wavelet-coherence). The meteorological dataset can be obtained from the China Meteorological Administration.

Author contributions

WH wrote the paper, did the Matlab code development, and analyzed the data. Both authors conceived the study, interpreted the results, and revised the paper.

Competing interests

The authors declare that they have no conflict of interest.

Acknowledgements

The preparation of this manuscript was supported by The New Zealand Institute for Plant and Food Research Limited under the Sustainable Agro-ecosystems programme.

References

Abramovich, F. and Benjamini, Y.: Adaptive thresholding of wavelet coefficients, Computational Statistics & Data Analysis, 22, 351-361, 1996.

Aloui, C., Hkiri, B., Hammoudeh, S., and Shahbaz, M.: A multiple and partial wavelet analysis of the oil price, inflation, exchange rate, and economic growth nexus in Saudi Arabia, Emerging Markets Finance and Trade, 54, 935-956, 2018.

Altarturi, B. H., Alshammari, A. A., Saiti, B., and Erol, T.: A three-way analysis of the relationship between the USD value and the prices of oil and gold: A wavelet analysis, AIMS Energy, 6, 487, 2018a.

Altarturi, B. H. M., Alshammari, A. A., Saiti, B., and Erol, T.: A three-way analysis of the relationship between the USD value and the prices of oil and gold: A wavelet analysis, Aims Energy, 6, 487-504, 2018b.

Biswas, A. and Si, B. C.: Identifying scale specific controls of soil water storage in a hummocky landscape using wavelet coherency, Geoderma, 165, 50-59, 2011.

Centeno, L. N., Hu, W., Timm, L. C., She, D. L., Ferreira, A. D., Barros, W. S., Beskow, S.,

558 and Caldeira, T. L.: Dominant Control of Macroporosity on Saturated Soil Hydraulic
559 Conductivity at Multiple Scales and Locations Revealed by Wavelet Analyses, Journal of
560 Soil Science and Plant Nutrition, 20, 2020.
561 Das, N. N. and Mohanty, B. P.: Temporal dynamics of PSR-based soil moisture across
562 spatial scales in an agricultural landscape during SMEX02: A wavelet approach, Remote
563 Sensing of Environment, 112, 522-534, 2008.
564 Graf, A., Bogena, H. R., Drüe, C., Hardelauf, H., Pütz, T., Heinemann, G., and Vereecken,
565 H.: Spatiotemporal relations between water budget components and soil water content in a
566 forested tributary catchment, Water Resour Res, 50, 4837-4857, 2014.
567 Grinsted, A., Moore, J. C., and Jevrejeva, S.: Application of the cross wavelet transform
568 and wavelet coherence to geophysical time series, Nonlinear Processes in Geophysics, 11,
569 561-566, 2004.
570 Gu, X. F., Sun, H. G., Tick, G. R., Lu, Y. H., Zhang, Y. K., Zhang, Y., and Schilling, K.:
571 Identification and Scaling Behavior Assessment of the Dominant Hydrological Factors of
572 Nitrate Concentrations in Streamflow, J Hydrol Eng, 25, 06020002, 2020.
573 Hargreaves, G. H.: Accuracy of estimated reference crop evapotranspiration, Journal of
574 irrigation and drainage engineering, 115, 1000-1007, 1989.
575 Hu, W., Chau, H. W., Qiu, W. W., and Si, B. C.: Environmental controls on the spatial
576 variability of soil water dynamics in a small watershed, J Hydrol, 551, 47-55, 2017a.
577 Hu, W. and Si, B. C.: Technical note: Multiple wavelet coherence for untangling scale-
578 specific and localized multivariate relationships in geosciences, Hydrol Earth Syst Sc, 20,
579 3183-3191, 2016.

580 Hu, W., Si, B. C., Biswas, A., and Chau, H. W.: Temporally stable patterns but seasonal
581 dependent controls of soil water content: Evidence from wavelet analyses, Hydrol Process,
582 31, 3697-3707, 2017b.
583 Jia, X., Zha, T., Gong, J., Zhang, Y., Wu, B., Qin, S., and Peltola, H.: Multi-scale dynamics
584 and environmental controls on net ecosystem CO_2 exchange over a temperate semiarid
585 shrubland, Agricultural and Forest Meteorology, 259, 250-259, 2018.
586 Kenney, J. F. and Keeping, E. S.: Mayhematics of Statistics, D. van Nostrand, 1939.
587 Koopmans, L. H.: The spectral analysis of time series, Elsevier, 1995.
588 Lakshmi, V., Piechota, T., Narayan, U., and Tang, C.: Soil moisture as an indicator of
589 weather extremes, Geophysical research letters, 31, L11401, 2004.
590 Li, H., Dai, S., Ouyang, Z., Xie, X., Guo, H., Gu, C., Xiao, X., Ge, Z., Peng, C., and Zhao,
591 B.: Multi-scale temporal variation of methane flux and its controls in a subtropical tidal salt
592 marsh in eastern China, Biogeochemistry, 137, 163-179, 2018.
593 Li, Z.: Applicability of simple estimating method for reference crop evapotranspiration in
594 Loess Plateau, Transactions of the Chinese Society of Agricultural Engineering, 28, 106-
595 111, 2012.
596 Mares, I., Mares, C., Dobrica, V., and Demetrescu, C.: Comparative study of statistical
597 methods to identify a predictor for discharge at Orsova in the Lower Danube Basin,
598 Hydrological Sciences Journal, 65, 371-386, 2020.
599 Mihanović, H., Orlić, M., and Pasarić, Z.: Diurnal thermocline oscillations driven by tidal
600 flow around an island in the Middle Adriatic, Journal of Marine Systems, 78, S157-S168,
601 2009.

602 Mutascu, M. and Sokic, A.: Trade openness-CO_2 emissions nexus: a wavelet evidence from
603 EU, Environmental Modeling & Assessment, 25, 1-18, 2020.
604 Nalley, D., Adamowski, J., Biswas, A., Gharabaghi, B., and Hu, W.: A multiscale and
605 multivariate analysis of precipitation and streamflow variability in relation to ENSO, NAO
606 and PDO, J Hydrol, 574, 288-307, 2019.
607 Ng, E. K. and Chan, J. C.: Geophysical applications of partial wavelet coherence and
608 multiple wavelet coherence, Journal of Atmospheric and Oceanic Technology, 29, 1845-
609 1853, 2012a.
610 Ng, E. K. and Chan, J. C.: Interannual variations of tropical cyclone activity over the north
611 Indian Ocean, International Journal of Climatology, 32, 819-830, 2012b.
612 Polansky, L., Wittemyer, G., Cross, P. C., Tambling, C. J., and Getz, W. M.: From moonlight
613 to movement and synchronized randomness: Fourier and wavelet analyses of animal
614 location time series data, Ecology, 91, 1506-1518, 2010.
615 Rathinasamy, M., Agarwal, A., Parmar, V., Khosa, R., and Bairwa, A.: Partial wavelet
616 coherence analysis for understanding the standalone relationship between Indian
617 Precipitation and Teleconnection patterns, arXiv preprint arXiv:1702.06568, 2017. 2017.
618 Schaefli, B., Maraun, D., and Holschneider, M.: What drives high flow events in the Swiss
619 Alps? Recent developments in wavelet spectral analysis and their application to hydrology,
620 Adv Water Resour, 30, 2511-2525, 2007.
621 Schulte, J., Duffy, C., and Najjar, R.: Geometric and topological approaches to significance
622 testing in wavelet analysis, Nonlinear Processes in Geophysics, 22, 2015.
623 Sen, A., Chaudhury, P., and Dutta, K.: On the co-movement of crude, gold prices and stock

index in Indian market, arXiv preprint arXiv:1904.05317, 2019. 2019.

Shen, X., Huang, H.-C., and Cressie, N.: Nonparametric hypothesis testing for a spatial signal, Journal of the American Statistical Association, 97, 1122-1140, 2002.

Si, B. C.: Spatial scaling analyses of soil physical properties: A review of spectral and wavelet methods, Vadose Zone Journal, 7, 547-562, 2008.

Si, B. C. and Farrell, R. E.: Scale-dependent relationship between wheat yield and topographic indices: A wavelet approach, Soil Sci Soc Am J, 68, 577-587, 2004.

Si, B. C. and Zeleke, T. B.: Wavelet coherency analysis to relate saturated hydraulic properties to soil physical properties, Water Resour Res, 41, W11424, 2005.

Song, X. M., Zhang, C. H., Zhang, J. Y., Zou, X. J., Mo, Y. C., and Tian, Y. M.: Potential linkages of precipitation extremes in Beijing-Tianjin-Hebei region, China, with large-scale climate patterns using wavelet-based approaches, Theoretical and Applied Climatology, 141, 1251-1269, 2020.

Su, L., Miao, C., Duan, Q., Lei, X., and Li, H.: Multiple‐wavelet coherence of world's large rivers with meteorological factors and ocean signals, Journal of Geophysical Research: Atmospheres, 124, 4932-4954, 2019.

Szolgayová, E., Arlt, J., Blöschl, G., and Szolgay, J.: Wavelet based deseasonalization for modelling and forecasting of daily discharge series considering long range dependence, J Hydrol Hydromech, 62, 24-32, 2014.

Tan, X., Gan, T. Y., and Shao, D.: Wavelet analysis of precipitation extremes over Canadian ecoregions and teleconnections to large‐scale climate anomalies, Journal of Geophysical Research: Atmospheres, 121, 14469-14486, 2016.

Torrence, C. and Compo, G. P.: A practical guide to wavelet analysis, Bulletin of the American Meteorological society, 79, 61-78, 1998.

Wendroth, O., Alomran, A. M., Kirda, C., Reichardt, K., and Nielsen, D. R.: State-Space Approach to Spatial Variability of Crop Yield, Soil Sci Soc Am J, 56, 801-807, 1992.

Westfall, P. H. and Young, S. S.: Resampling-based multiple testing: Examples and methods for p-value adjustment, John Wiley & Sons, 1993.

Wu, K., Zhu, J., Xu, M., and Yang, L.: Can crude oil drive the co-movement in the international stock market? Evidence from partial wavelet coherence analysis, The North American Journal of Economics and Finance, 2020. 101194, 2020.

Yan, R. and Gao, R. X.: A tour of the tour of the Hilbert-Huang transform: an empirical tool for signal analysis, IEEE Instrumentation & Measurement Magazine, 10, 40-45, 2007.

Zhao, R., Biswas, A., Zhou, Y., Zhou, Y., Shi, Z., and Li, H.: Identifying localized and scale-specific multivariate controls of soil organic matter variations using multiple wavelet coherence, Sci Total Environ, 643, 548-558, 2018.